pubs.acs.org/estengg

Article

Engineering Calcium-Bearing Mineral/Hydrogel Composites for Effective Phosphate Recovery

Albern X. Tan, Elizabeth Michalski, Jan Ilavsky, and Young-Shin Jun*

Cite This: https://doi.org/10.1021/acsestengg.1c00204

Read Online

ACCESS | Metrics & More | Article Recommendations | Supporting Information

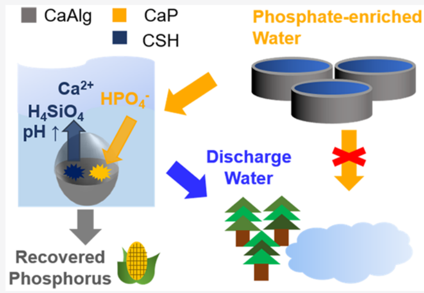

ABSTRACT: Effectively recovering phosphate from wastewater streams and reutilizing it as a nutrient will critically support sustainability. Here, to capture aqueous phosphate, we developed novel mineral−hydrogel composites composed of calcium alginate, calcium phosphate (CaP), and calcium silicate hydrate (CSH) (CaP + CSH/Ca-Alg). The CaP + CSH/Ca-Alg composites were synthesized by dripping a sodium alginate (Na-Alg) solution with ionic precursors into a calcium chloride bath. To change the mineral seed's properties, we varied the calcium bath concentrations and the ionic precursor (sodium dibasic phosphate (NaH_2PO_4) and/or sodium silicate (Na_2SiO_3)) amounts and their ratios. The added CSH in the mineral−hydrogel composites resulted in the release of calcium and silicate ions in phosphate-rich solutions, increasing the saturation ratio with respect to calcium phosphate within the mineral−hydrogel composites. The CSH addition to the mineral−hydrogel composites doubled the phosphate removal rate while requiring lesser initial amounts of Ca and P materials for synthesis. By incorporating both CSH and CaP mineral seeds in composites, we achieved a final concentration of 0.25 mg-P/L from an initial 6.20 mg-P/L. Moreover, the mineral−hydrogel composites can remove phosphate even under CaP undersaturated conditions. This suggests their potential to be a widely applicable and environmentally sustainable treatment and recovery method for nutrient-rich wastewater.

KEYWORDS: *Hydrogel, Calcium Phosphate, Calcium Silicate Hydrate, Calcium Alginate, Mineral Growth*

■ INTRODUCTION

Anthropogenic phosphorus (P) pollution originates from both point sources (e.g., wastewater treatment plants or industrial effluents)[1] and nonpoint sources (e.g., agricultural runoff),[2] and is one of the primary drivers of eutrophication. Eutrophication drives harmful algal blooms that release cyanobacterial toxins, which can threaten public health and harm industries such as fisheries or tourism. For example, in a 2015 report, the United States Environmental Protection Agency estimated a loss of \$37 million to \$47 million in tourism revenue over two years due to an algal bloom in an Ohio lake and a loss of \$2.5 million in fisheries revenue in Maine due to one harmful algal bloom.[3] Spurred by such losses, much effort has been made to limit eutrophication by reducing the loading of nutrients in surface waters. Effective P management is especially important, because considerable evidence implicates it as the limiting nutrient for harmful algal blooms.[4] On the supply side, P mining costs are increasing, and most phosphate rock sources are geographically concentrated, thus presenting accessibility challenges. Furthermore, the increasing global population is consuming more P. All these factors that motivate effective P recovery from waste streams and its reuse.[5,6]

A promising method for nutrient recovery from high concentration phosphate-containing wastewater is crystallization, which recovers nutrients by forming solids, such as struvite ($MgNH_4PO_4$) or calcium phosphate (CaP).[7−9] Previously, struvite formation and recovery has been heavily studied, and pilot plants and full-scale applications are already being implemented.[8,9] However, struvite precipitation can be impeded by common wastewater constituents, such as calcium or bicarbonate, and require chemical feedstocks, such as magnesium chloride.[7,10] CaP precipitation is also advantageous for phosphorus recovery, owing to the abundance of calcium in natural waters and the chemical similarity of CaP to typical phosphate rock sources.[8] Commonly, to induce CaP precipitation, calcium chloride, calcium hydroxide, or lime are used as supplementary calcium sources. In such processes, nucleation is usually the rate-determining step for CaP precipitation;[11−13] thus, an additional pH adjustment to alkaline pH values (>10) or an adjustment to $[Ca^{2+}]$ concentration can also be necessary to induce fast CaP precipitation by increasing the thermodynamic driving force. Because of the required high pH value, simultaneous formation of calcium carbonate can also lower the overall purity of the

Received: June 5, 2021
Revised: August 3, 2021
Accepted: August 4, 2021

final product.[9] In addition, CaP precipitates exhibit low settleability and can be difficult to collect due to their small sizes.[13−15]

The removal of phosphorus through crystallization can be improved by implementing "seed" materials, which are generally applied as suspended powders in solution to act as substrates for mineral growth. Seed materials for struvite, such as preformed struvite crystals, increase the overall recovery efficiency, kinetics, and final particle size. To form CaP, a variety of seed materials have been suggested, such as calcite[16] or calcium silicate minerals.[15,17,18] Seed materials benefit the CaP crystallization process by increasing the kinetics of the process or by buffering or changing aqueous conditions to favor CaP formation.[8,9]

Using CaP as a seed mineral, we previously developed CaP/calcium alginate (Ca-Alg) mineral−hydrogel composites.[19] During gelation, Ca-Alg formation is accompanied by CaP mineral seed formation *in situ*. This method distributes the CaP seed throughout the hydrogel matrix while circumventing the generally high-energy mixing step required to evenly disperse nanoparticles in a hydrogel precursor matrix. Based on low solubility of CaP, this composite was able to remove and recover P effectively (from 6.2 mg-phosphorus/L (mg-P/L) to 0.7 mg-P/L in ∼22 h, with a loading capacity of 96.4 mg-P/g CaP mineral seed). Furthermore, compared to other nanometer or micrometer sized seed materials, the ∼2 mm size of the mineral−hydrogel composite facilitates easier separation and collection from solution. Implementing the CaP seeds also lowers the high energy barrier for CaP formation, prompting the formation of CaP from solutions. CaP/Ca-Alg composites can be applied for recovery and removal of phosphorus from water containing excess phosphate. While this approach is highly advantageous, a few improvements can be made: For one, the kinetics of phosphorus removal using this technique are slower than in traditional adsorption processes or crystallization from highly supersaturated solutions, which typically reach equilibrium within 1−4 h.[20] The process is also dependent on the aqueous chemistry of the target waterbody and, therefore, is not applicable to soft waters or to waters with a pH < 7, where the solubility of calcium phosphate increases as pH decreases. To improve these aspects, in our new approach presented here, we mixed soluble phosphate (P) and silicate (Si) in a sodium alginate precursor solution. Then, during gelation in a calcium chloride bath, the calcium interacted and formed CaP and calcium silicate hydrate (CSH) seed minerals while simultaneously cross-linking the alginate. We then applied these mineral−hydrogel composites for P removal and recovery. Based on previous work, CSH-based mineral seeds applied as powder suspension were shown to improve phosphorus recovery by releasing Ca^{2+} and simultaneously increasing the pH of the solution.[21] Hence, we expected that our engineered mineral−hydrogel composites containing both CaP and CSH would synergistically act to recover phosphorus from our chosen aqueous conditions, improving the kinetics and applicability of the Ca-mineral/hydrogel composites and demonstrating their promise as a novel phosphate removal and recovery method.

Therefore, the goals of this study were to synthesize novel calcium mineral−hydrogel composites that enable fast and broadly applicable P removal and recovery and to investigate their working mechanisms. To accomplish this, we incorporated CSH into our previously reported CaP/Ca-Alg mineral−hydrogel composites.[19] We then compared the P-removal/recovery performance of (1) CaP only containing mineral−hydrogel composites, (2) CSH containing mineral−hydrogel composites, and (3) CaP + CSH containing mineral−hydrogel composites to determine the mineral seeds' individual and synergistic effects. Furthermore, we examined the effect of varying the calcium bath concentration. The calcium bath concentration directly affected the mineral seed's characteristics and its subsequent P recovery ability. However, the large amount of calcium necessary for the process made it one of the largest sources of cost for the composites. Therefore, we also examined whether adding Si can lower the material synthesis requirements, improving the resource-use efficiency. Finally, we elucidated the underpinning mechanisms of phosphorus removal and recovery, especially the effect of the hydrogel system on the P removal and recovery performance and the presence of silicate during both the synthesis and the application of the mineral−hydrogel composites. The findings here demonstrated the potential of CaP + CSH/CaAlg as a new phosphate removal and recovery technology that utilizes green chemistry principles.

EXPERIMENTAL SECTION

Materials. Sodium silicate solution (Reagent grade) was purchased from Sigma-Aldrich. Its concentrations were measured by an inductively coupled plasma optical emission spectroscopy (Optima 7300DV) (ICP-OES). Sodium alginate (FCC grade) was purchased from Spectrum Chemicals. All other chemicals used were at least ACS grade. Deionized (DI) water (≥18.1 MΩ·cm) was obtained using a Barnstead Nanopure Diamond Ultrapure water system.

Fabrication of Mineral−Hydrogel Composites. A 0.6% (w/w) sodium alginate solution, with ionic precursors of sodium silicate for silicate (Si) or sodium dihydrogen phosphate for phosphate (P), was dripped into calcium chloride gelation baths with calcium concentrations of 180 mM, 90 mM, 45 mM, and 22.5 mM, and 20 mM NaOH (at a pH of ∼11.7). The sodium alginate drip was driven by a syringe pump at a rate of 5 mL/min from a height of 10 cm above the bath, with magnetic stirring at 400 rpm. The calcium concentrations and synthesis conditions were chosen after pretests to determine what calcium concentrations and conditions successfully form mineral−hydrogel composites in the form of spherical beads of consistent and uniform sizes (Figure 1). The resulting hydrogel beads were soaked in the calcium chloride bath for 4 h and then washed with DI water three times to remove unreacted precursors.

Characterization of Mineral−Hydrogel Composites. After washing, mineral−hydrogel composites were patted to remove extra water and weighed to determine their wet weight. They were then dried for 24 h in a 40 °C incubator and weighed again to determine their dry weight. To image the mineral seeds, mineral−hydrogel composites were dehydrated in pure ethanol and then, while still swollen with ethanol, ground in a mortar and pestle to fragment the hydrogel structure and allow clear imaging of the mineral seed. Afterward, the sample was allowed to air-dry at room temperature, and the resulting powder was imaged with a scanning electron microscope equipped with a backscattering electron detector (Thermofisher Quattro S E-SEM, SEM-BSE). Energy dispersive X-ray (EDS) spectroscopy measurements of the composites were simultaneously collected (Oxford Instruments EDS detector). ImageJ 1.8 was used to measure the mineral−hydrogel composite sizes and the

https://doi.org/10.1021/acsestengg.1c00204
ACS EST Engg. XXXX, XXX, XXX−XXX

mineral seed sizes from the SEM-BSE images.[22] Multiple sites of the powders were imaged, and representative images are presented in Figure 2 and Figures S2, S3, and S4 in the Supporting Information (SI).

To characterize the mineral seeds' sizes and mineral phases, synchrotron-based ultrasmall angle X-ray scattering (USAXS) (q = 0.0001−0.3 Å^{-1}), small-angle X-ray scattering (SAXS) (q = 0.05−1.2 Å^{-1}), and wide-angle X-ray scattering (WAXS) (q = 1.0−6.0 Å^{-1}) patterns were collected at beamline 9-ID-C[23−25] at the Advanced Photon Source (APS) at Argonne National Laboratory, IL. Hydrogel samples were prepared in 4 mm internal diameter glass NMR sample tubes closed at one end with a length of 55 mm (Wilmad Lab Glass). The hydrogel precursor solution (0.1 mL) was placed into the glass tube using a 28-gauge needle. The calcium chloride solution was then pipetted into the glass tube (0.5 mL), and the tube was submerged vertically in the gelation bath for 8 h. Afterward, the tube was submerged vertically in DI water for 1 h to remove unreacted precursors. The interface of the hydrogel was found visually (Figure S1A in the SI). Scans were taken down from the interface in three distinct regions, 0−200 μm below the hydrogel surface, 200−400 μm below the hydrogel surface, and 400−600 μm below the surface (Figure S1B,C in the SI). Three samples were measured for each different mineral seed conditions. Every sample scan was used (3 scans per sample, 3 samples per condition) for particle size fitting (USAXS) and peak identification (WAXS). The beam size was 200 μm × 200 μm, and the beam energy was 21 keV. USAXS, SAXS, and WAXS patterns were collected from the same spot. Scattering data was processed with various macros in Nika and Irena packages written for Igor Pro (Wavemetrics, Lake Oswego, OR, U.S.A.) developed by Dr. Jan Ilavsky.[25] The use of three different detectors at beamline 9-ID-C allowed for the collection of X-ray scattering data from q values ranging from 0.0001 to 6 Å^{-1}. The USAXS measurements were done with a photodiode detector, and the SAXS and WAXS measurements were conducted with a Pilatus 100 K detector and a modified Pilatus 300 K-W detector. Triplicate samples were measured and used for the sample analysis. Representative WAXS and USAXS data are presented in Figures 1B and 2B, respectively. A more detailed discussion of the sample setup and measurement for X-ray scattering data analysis and measurement is available in the SI (Section S3 in the SI).

Phosphate Removal Experiments. To test the P removal performance, a P-rich solution containing the main ionic precursors involved in CaP precipitation with an adjusted ionic strength (2 mM $CaCl_2$, 0.2 mM Na_2HPO_4, and 30 mM NaCl, at initial pH 7.0) was used (saturation index with respect to hydroxyapatite = 6.95). These concentrations are typical values for dissolved calcium, phosphate, and ionic strength in secondary effluents.[26] In particular, we chose this phosphate concentration as a compromise between high phosphate containing wastewaters (e.g., the side streams of a wastewater treatment plant (∼10 mM soluble P)[27] and low phosphate containing wastewaters (e.g., wastewater effluent without any targeted tertiary treatment for phosphorus removal (∼0.03 mM P).[28] The saturation index is defined as $\log_{10}(\mathrm{IAP}/K_{sp})$, where IAP is the ion activity product with respect to hydroxyapatite ($Ca_5(PO_4)_3(OH)_1$) and K_{sp} is the solubility product of hydroxyapatite ($10^{-44.33}$ in the thermo.vdb database file). The saturation index was calculated by Visual MINTEQ (Version 3.1) using the thermo.vdb database. After mineral−hydrogel composites were added to the solution, the batch reaction was allowed to proceed for 16 h under stirring. The mineral−hydrogel composite amount was fixed at 5 mL of precursor solution, and the P-rich solution volume was set at 200 mL. Afterward, filtered (0.2 μm pore size) samples were taken. Additionally, after removing the mineral−hydrogel composites, we determined the amount of homogeneous CaP nucleation and growth in the solution by adding 100 μL of 1% nitric acid to dissolve CaP particles for analysis. Calcium, silicate, and phosphate concentrations were determined using ICP-OES. The partitioning of the initially dissolved P after the reaction was determined by three quantities: (1) the amount of phosphate remaining in the solution (dissolved) (P_{diss}), (2) the amount of phosphate removed by the mineral−hydrogel composites through heterogeneous nucleation and mineral growth in the composites (P_{Het}), and (3) the amount of phosphate that homogeneously nucleated and grew to form CaP precipitates in the solution (P_{Hom}). P_{Diss} was determined by collecting filtered samples using 0.22 μm pore size filters. P_{Hom} was determined by measuring the P concentration after acidifying the reaction solution with 1% nitric acid after filtration. The mineral−hydrogel composites were physically removed using a metal mesh (approximately US mesh size 18) before acidification. P_{diss} was then subtracted from the total amount of dissolved P after acidification to determine the amount of CaP precipitate in the solution. P_{Het} was determined by subtracting the sum of P_{Diss} and P_{Hom} from the initial amount of P in the solution. In the figures here, P_{Het} is labeled "P in MinHG", P_{Hom} is labeled "CaP in solution", and P_{Diss} is labeled "Dissolved". The CaP mineral formation within the mineral−hydrogel composites is referred to as heterogeneous CaP nucleation and growth, because either the hydrogel or the mineral seed acts as a substrate that CaP can form on.

To determine the kinetics of P removal, reactions under identical conditions were also run, with 5 mL of sample being taken at doubling time points: 0, 30 min, 1 h, 2 h, 4 h, 8 h, and 16 h. To determine the solubility and mechanisms of P removal, similar reactions were also carried out in 30 mM NaCl solution at initial pH = 7 and in solutions undersaturated with respect to hydroxyapatite (0.2 mM Na_2HPO_4, 30 mM NaCl, at initial pH = 7) and having the same composite amount and reaction volume. To determine the effect of common anions on the P recovery and removal performance of the CaP + CSH/CaAlg mineral−hydrogel composites, we modified the model aqueous solution to contain (1) 1 mM sodium nitrate and 1 mM sodium sulfate or (2) 1 mM sodium nitrate, 1 mM sodium sulfate, and 2 mg-C/L dissolved organic matter (DOM). For DOM, we utilized Suwanee River Natural Organic Matter (2R101N) which was purchased from the International Humic Substance Society (IHSS). The DOM concentration from SRNOM stock solution was confirmed using a nonpurgeable total organic carbon measurement (NPOC, Shimadzu TOC Analyzer, TOC-L CPH). To measure the phosphate concentrations in solutions containing DOM, the molybdenum blue method was used. Specifically, 880 nm absorbances using a UV−visible spectrometer (Thermo Scientific Evolution 60S UV−visible spectrophotometer) were used to calculate phosphate concentrations. All experiments were performed in triplicate. A summary of the experimental goals and conditions are found in Table S1 in the SI.

https://doi.org/10.1021/acsestengg.1c00204
ACS EST Engg. XXXX, XXX, XXX−XXX

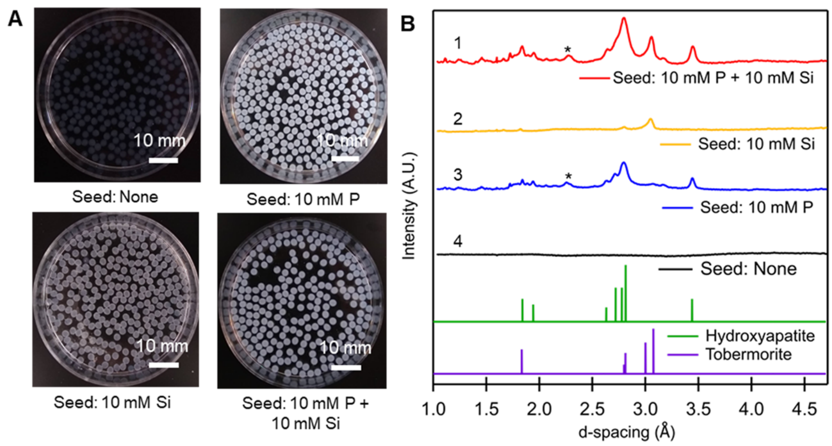

Figure 1. (A) Pictures of mineral−hydrogel composites made with each different mineral seed. (B) Reference wide-angle X-ray spectra (WAXS) and representative sample WAXS spectra. Each spectrum has the same intensity scale (*y*-axis), allowing for direct comparison of crystallinities. Calcite peaks are marked with *. The scans shown here were taken from a depth of 400−600 μm in the hydrogel samples prepared for X-ray scattering characterization.

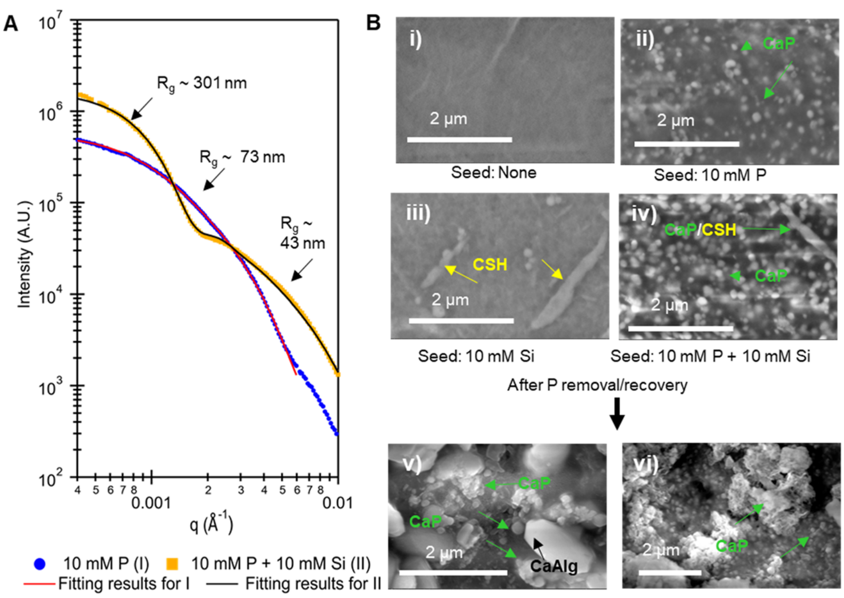

Figure 2. (A) Ultrasmall angle X-ray scattering results and their fittings for different mineral seeds. (B) SEM images of the different mineral−hydrogel composites. Yellow or green arrows indicate examples of the mineral seeds. The corresponding colored text is its composition as determined by EDS (Figure S2). In (B), ii, iv, v, and vi, green arrows indicate CaP containing particles and aggregates before and after the P recovery reaction for 10 mM Si and 10 mM P + 10 mM Si seeded mineral−hydrogel composites, identified using SEM-EDS (Figure S2). The black arrow indicates that the large solid features were determined to be the calcium alginate hydrogel (Figure S3).

RESULTS AND DISCUSSION

Synthesis and Characterization of Mineral−Hydrogel Composites. After the sodium alginate and ionic precursor solutions were dripped into the calcium chloride bath, they formed spherical hydrogel beads (shown suspended in water in Figure 1A). If ionic precursors were included in the sodium alginate solution, the hydrogel bead quickly turned opaque, indicating mineral seed formation. After synthesis, the dry weights of the mineral−hydrogel composites were measured to confirm the formation of and quantify the mineral seed formed (Table S2). The CaP seeds and CSH seeds formed similar weights of mineral, with the two mineral seeds making up ∼29% of the total dry weight. The CaP + CSH seeds together accounted for ∼44% of the total dry weight. Overall, as expected, the combined CaP + CSH seeds formed about twice as much mineral seed weights as the CaP and CSH seeds, based on their dry weight. For example, the mineral seed weights were 25 mg for CaP + CSH, compared to ∼13 mg and ∼16 mg for CSH only and CaP only, respectively. The hydrogel bead sizes were similar (∼2 mm diameter) and showed no observable difference among the various mineral seeds. Detailed weights and hydrogel sizes can be found in Table S2 in the SI.

Hydrogel samples were measured with USAXS and WAXS at APS beamline 9-ID-C. USAXS measured the mineral seed's morphology and particle size in the composites, while WAXS identified the mineral phase present in the composites. Standard mineral peaks were referenced from the Mindat database.[29] WAXS scattering patterns (Figure 1B) showed that the CaP seeds formed phases similar to hydroxyapatite, showing major peaks at *d*-spacings of ∼2.8 and 3.4 Å (Spectrum 3 in Figure 1B). CSH seeds displayed peaks similar

https://doi.org/10.1021/acsestengg.1c00204
ACS EST Engg. XXXX, XXX, XXX−XXX

to those of tobermorite, a naturally occurring CSH mineral, indicated by major peaks at d-spacings of ~1.8, 2.8, and ~3.0 Å (Spectrum 2 in Figure 1B). In the combined seed cases, both mineral phases were observed (Spectrum 1 in Figure 1B). In addition, a peak around ~2.3 Å was attributed to calcite (marked with *), which may have formed owing to the high calcium concentration and high pH conditions in the calcium bath (Spectra 1 and 3 in Figure 1B). These results are similar to those recently reported by Solonenko et al., who studied precipitation in an aqueous system containing Ca−Si−P for application as a bioceramic material for bone regeneration.[30] Interestingly, instead of tobermorite, they reported clear calcite XRD peaks as the result of Si incorporation. In our study, we mainly observed peaks associated with tobermorite (Spectra 1 and 2 in Figure 1B). In another report regarding a Ca−P−Si precipitation system, Mostafa et al. found only hydroxyapatite peaks.[31] Their study examines the simultaneous increased incorporations of silicate and carbonate into the HAP structure during precipitation of $Ca(OH)_2$, NaH_2PO_4, and Na_4SiO_4 in solution without the presence of alginate. On the other hand, in our system, while some carbonate substitution may have occurred, clear peaks in Spectrum 1 of Figure 1B can be attributed to CSH, suggesting that the dominant mineral phase in Si-containing systems is tobermorite. Overall, our method of coprecipitation during gel formation was able to produce mineral−hydrogel composites seeded with CSH or CaP + CSH without a large amount of calcite or carbonate impurities, limiting their roles in inhibition of CaP nucleation and growth during P recovery.[32]

USAXS scattering patterns (Figure 2A) revealed that the mineral seed morphology and particle size were different for each different mineral seed. The CaP seeded system had one primary particle size distribution with a radius of gyration (R_g) ~ 73 ± 2 nm (three replicates). Assuming a spherical shape, the relation between R_g and the particle diameter is $R_g^2 = R^2 \cdot (3/5)$. Therefore, the CaP seeded system had an estimated diameter (D) of ~190 nm. Scattering at lower q revealed that the primary particles may have associated in mass fractal aggregates with a dimension of ~2.4, indicating that they are relatively densely packed.[33] The CaP + CSH seeded hydrogels had two main particle sizes (R_{g1} and R_{g2}), with R_{g1} ~ 301 ± 36 nm and R_{g2} ~ 43 ± 14 nm (three replicates). Once again assuming a spherical particle, these radii correspond to D_1 ~ 780 nm and D_2 ~ 93 nm. For the CSH seeded hydrogel, the contrast in electron density between the mineral seed and the surrounding water/hydrogel matrix was not high enough for USAXS to clearly determine the particle size and morphology. Therefore, the measured USAXS patterns for CSH/Ca-Alg were not used.

To verify our interpretation of the USAXS patterns, complementary SEM-EDS analyses were conducted. For this measurement, we dehydrated the hydrogels in ethanol and ground them in a mortar and pestle. The grinding of the hydrogel beads created freely floating hydrogel fragments that, when imaged, clearly showed the mineral seeds (Figure 2B). Imaging a hydrogel without a mineral seed revealed a smooth dried hydrogel surface (Figure 2B i). Imaging the 10 mM P mineral−hydrogel composites revealed spherical particles with diameters of 104 nm ± 27 nm (n = 81), and their SEM-EDS analysis indicated that the mineral particles are CaP (Figure S2B ii in the SI). Imaging of the 10 mM Si mineral seeded composites with SEM-EDS (Figure 2B iii and Figure S2C in the SI) revealed a large size range of CSH particles. Finally, the 10 mM P + 10 mM Si mineral seeds in hydrogels were comprised of similarly sized small spherical particles (diameters of 137 nm ±27 nm (analyzed particle numbers = 66)) with larger irregularly shaped particles with dimensions of ~1 μm (Figure 2B iv and red boxes in Figure S4 in the SI). Their SEM-EDS analysis identified the small spherical particles as mainly CaP, with some small silicate impurities, while the larger particles were a mix of CaP and CSH (3% atomic phosphorus and 1.5% atomic silica) (Figure S2D in the SI). This suggests that the 10 mM P + 10 mM Si mineral seeds were formed through coprecipitation of CaP and CSH during calcium alginate hydrogel formation. The elemental composition of the mineral seed formed in this study was similar to that of the mineral aggregates precipitated from a Ca−Si−P system reported by Solonenko et al.[30] With regards to the mineral aggregate size, however, they reported that, regardless of silicate content, their mineral precipitates were comprised of aggregates sized from 3 to 100 μm. On the other hand, the CaP mineral seeds in our work were largely spherical single particles with submicrometer sizes. We attribute this difference to the presence of alginate polymers and the formation of Ca-Alg hydrogel during the initial stages of nucleation and growth of minerals. As a result, our mineral seeds were smaller, with a correspondingly larger surface areas and increased reactivities.

The mineral−hydrogel composites seeded with CSH and CaP + CSH mineral seeds were imaged after the P removal/recovery reaction in the P-rich solution. The CaP mineral seeds were not imaged because similar mineral seeds were imaged and reported in our previous work.[19] There, we found that CaP particles a few micrometers in size formed after the reaction, whereas only submicrometer CaP particles were observed before the reaction. The XRD patterns in our previous work showed that the CaP mineral seeds' phase did not change during the P-recovery reaction. For the CSH mineral seeds, phosphate containing aggregates were observed (Figure S3 in the SI). The large (micrometer scale) solid regions that were also observed did not contain large amounts of silicon or phosphorus, indicating that it was the calcium alginate matrix (magenta box in Figure S3). For the CaP + CSH seeded mineral−hydrogel composites, similar aggregates were observed. Spherical CaP particles with a similar size to the particles observed before the reaction are also still visible. Additionally, large micrometer scale solid particles in the top right of Figure S4B are observed that clearly contain CSH based on their elemental composition (Figure S4 in the SI). For the CSH mineral seeded composites, the presence of phosphorus after the reaction was clearly shown, while a decrease in silicate content was also observed. For the CaP + CSH mineral seed, the mineral compositions, as measured by SEM-EDS, were similar before and after the reaction. The recovered CaP minerals' phase, based on our previously reported results, is expected to be similar to its mineral phase before the reaction. These aggregates and mineral-seed particles are contained within the macroscale structure of the calcium alginate hydrogel and can be thus easily recovered from the solution due to the hydrogel's millimeter-scale size. The CaP containing aggregates and particles can thus be reused as a fertilizer or for other applications.

One caveat is that the mineral morphologies and sizes, especially of the CSH minerals, can be altered by drying. Thus, the particle size from the USAXS fitting and that was measured from the SEM-BSE images could differ. Drying can shrink hydrated particles, or alternatively, the same drying process can

https://doi.org/10.1021/acsestengg.1c00204
ACS EST Engg. XXXX, XXX, XXX−XXX

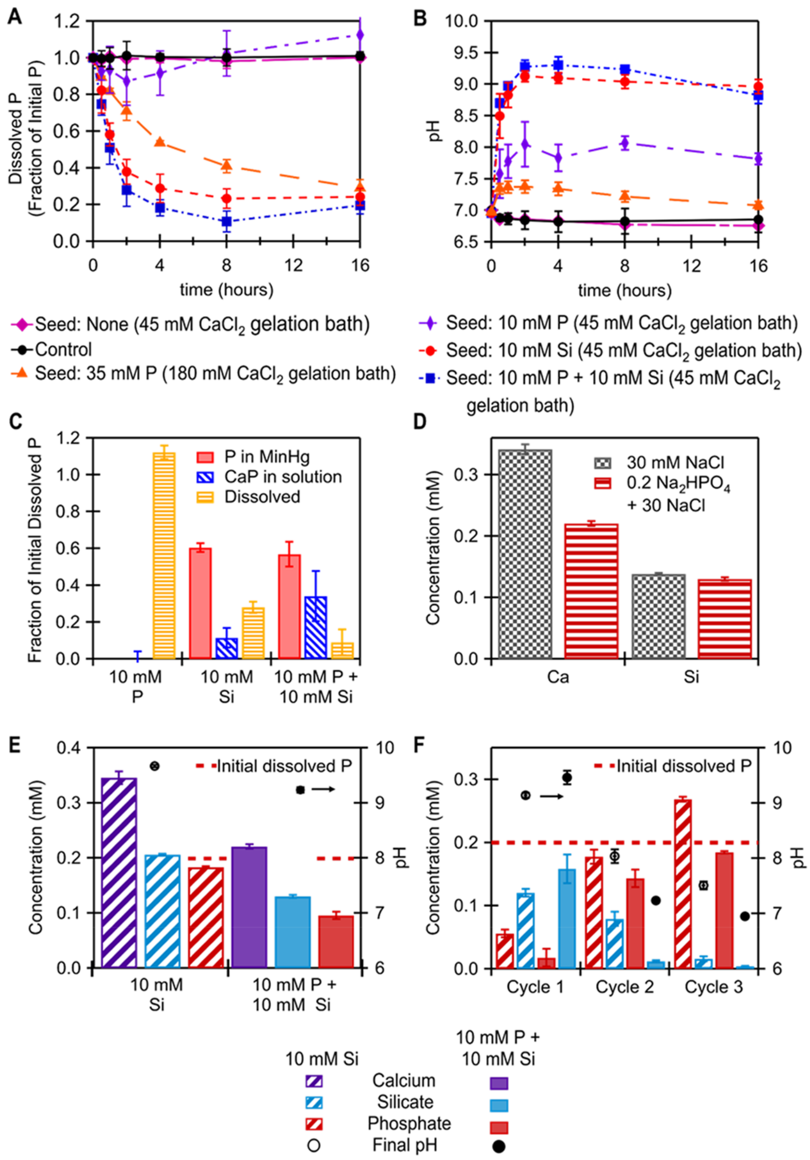

Figure 3. (A) Kinetics of dissolved phosphate in the P-rich solution system over time, when exposed to the different mineral−hydrogel composites. (B) pH change over time for the P-rich solution when exposed to different mineral−hydrogel composites. (C) Final distribution of phosphate in the system after 16 h. (D) Release of calcium and silicate from CaP + CSH/Ca-Alg in different reaction solutions after 16 h. (E) pH and final concentrations after a 16 h reaction in a solution undersaturated with respect to hydroxyapatite (0.2 mM Na_2HPO_4, 30 mM NaCl, initially at pH 7) for CaP + CSH mineral−hydrogel composites and CSH mineral seeded mineral mineral−hydrogel composites. (F) Final dissolved phosphate and silicate concentrations and final pH for CaP + CSH mineral and CSH mineral seeded hydrogel composites after repeated exposure to P-rich solutions (1 cycle is defined as 16 h reaction). The red dashed line is the original dissolved phosphate concentration before the reaction starts. All error bars are from triplicate samples and represent 1 standard deviation. Red arrows in (A), (C), and (E) indicate where dissolution of CaP mineral seed occurred.

cause aggregation of small particles that were originally dispersed in the hydrogel, making them appear larger.

Effects of Seed Compositions on P Removal: Comparison of P, Si, and Their Combinations. Mineral−hydrogel composites with different seed minerals were synthesized by changing the ionic precursor amounts in the sodium alginate solution before gelation in the $CaCl_2$ bath. The ionic precursors tested were 10 mM Na_2HPO_4 (CaP), 10 mM Na_2SiO_3 (CSH), or 10 mM Na_2HPO_4 + 10 mM Na_2SiO_3 (CaP + CSH). Their phosphate removal and recovery performances were then tested with the P-rich solution. For comparison, our previously reported formulation (0.6% (w/w) sodium alginate + 35 mM $NaHPO_4$, formed in a 180 mM $CaCl_2$ + 20 mM NaOH bath)[19] was also tested under identical conditions. Both the Ca-Alg hydrogel seeded with 10 mM Si and that with 10 mM Si + 10 mM P reached comparable final dissolved P values. Their P removal kinetics were twice as fast as those of our previous formulation:[19] they reached equilibrium in ∼8 h, as opposed to >16 h (Figure 3A). As expected, adding CSH seeds released soluble silicates and increased the pH (Figure 3B). In addition, phosphate removal and recovery with the CaP + CSH seeded Ca-Alg used less material than our previously reported formulation (25% of the original $CaCl_2$ and 28.5% of the original P amount necessary for the CaP seed). The pure CaP seed formed using the reduced P amount (10 mM P seed, which is 28.5% of the original P concentration (35 mM P)) did not remove phosphate effectively.

https://doi.org/10.1021/acsestengg.1c00204
ACS EST Engg. XXXX, XXX, XXX−XXX

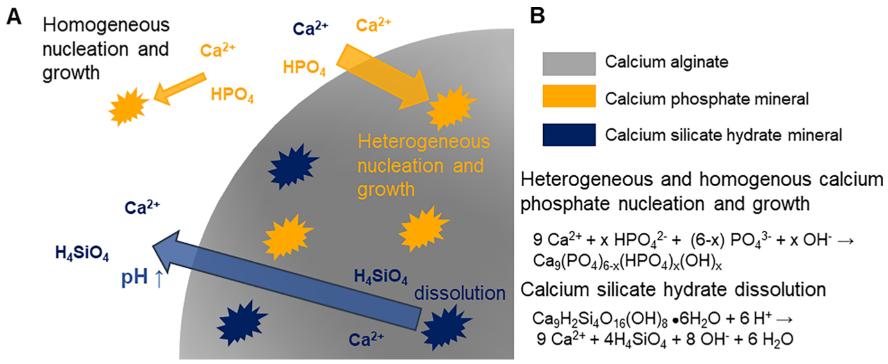

Figure 4. (A) Proposed mechanisms and (B) stoichiometric reactions governing calcium and silicate release, the increase in pH, and the removal and recovery of phosphate. The stoichiometric equation for CSH dissolution is based on ref 41 and our own estimate of the Ca:Si ratio (Figure 3D). The equation for amorphous CaP formation is from ref 40.

Phosphate was removed as either homogeneously nucleated and grown CaP particulates or, within the mineral–hydrogel composite, as heterogeneously nucleated and grown CaP mineral (Figure 3C). The homogeneous nucleation occurred due to the increase in pH and released [Ca^{2+}] induced by the dissolution of the CSH seeds. Thus, there is competition between the formation and growth of homogeneous CaP nuclei in solution and the uptake of [P] by heterogeneous nucleation within the mineral–hydrogel composites. Of the two nucleation types, the heterogeneously nucleated P is easily recovered from the mineral–hydrogel composites, while the homogeneously nucleated P is present in solution as aggregates of CaP mineral. However, the homogeneously nucleated P also contributes to a final low soluble P concentration. For example, reacting the CaP + CSH/Ca-Alg mineral–hydrogel composites in the model P-rich solution resulted in final concentrations as low as 0.018 mM phosphate (or 0.55 mg-P/L). By comparison, reacting the CSH/Ca-Alg mineral–hydrogel composite in the P-rich condition only reached a final P concentration of 0.056 mM phosphate (or 1.73 mg-P/L). Despite the CSH-only and CaP + CSH mineral–hydrogel composites removing similar amounts of P through heterogeneous nucleation (60.4% and 56.9% of the initial dissolved P for CaP + CSH and CSH, respectively, Figure 3C), the CaP + CSH mineral–hydrogel composites induced more homogeneous nucleation and reached lower final P concentrations. Therefore, both types of nucleation need to be considered in assessing the mineral-hydrogel composite's ability to remove and recover phosphate. Additionally, by increasing the dosage of the mineral–hydrogel composite, the combined mineral seed reached concentrations as low as 0.25 mg-P/L. phosphate.

In the P-rich solutions tested, as we mentioned above, comparable amounts of P were removed by heterogeneous nucleation on the CaP + CSH seeded mineral–hydrogel composites and the CSH seeded mineral–hydrogel composites (Figure 3C). The main difference was the homogeneously removed P fraction amount. However, the two mineral–hydrogel composites differed in other key regards: For one, the CaP + CSH mineral seeded composites released silicate more quickly than the CSH mineral seeded composites (Figure S5 in the SI). This quicker release contributes to the larger homogeneous nucleation fraction, as the quick release of Ca^{2+} increases the supersaturation ratio of CaP in the solution, promoting the homogeneous removal of P that occurs in parallel to the heterogeneous recovery of P. The CaP + CSH mineral seeded composites also have a higher ability to heterogeneously remove P. When the mineral–hydrogel composites were reacted in hydroxyapatite undersaturated solutions, the combined CaP + CSH seeded mineral–hydrogel composites recovered significantly more P than the CSH seeded mineral–hydrogel composites (Figure 3E). The CaP + CSH mineral seeded composites are also more stable that the CSH mineral seeded composites. When the mineral–hydrogel composites were reused in multiple cycles, the CaP + CSH mineral seeded composites did not release P, while the CSH mineral–hydrogel composite began leaching P (Figure 3F). Overall, the CaP + CSH mineral seeded composites have a higher affinity for heterogeneous P removal, making P recovery more expedient, and do not leach P as easily as the CSH mineral seeded composites, promoting their use.

Reaction of Mineral–Hydrogel composites in the P-Rich Solution: Mechanisms for P Removal and Recovery. To confirm the mechanism of P removal by the mineral–hydrogel composites, the calcium and silicate release from CaP + CSH seeded mineral–hydrogel composites was also tested in two additional solution conditions: (1) 30 mM NaCl and (2) 0.2 mM Na_2HPO_4 + 30 mM NaCl (under-saturated with respect to hydroxyapatite, SI = −59.3), both at initial pH = 7 (Figure 3D). The silicate release was found to be largely consistent whether P was present or not. With regard to calcium, the calcium release was much less when phosphate was present, indicating that P uptake was mainly accomplished by CaP mineral formation within the mineral–hydrogel composites (∼60% of initial P heterogeneously removed) (Figure S6 in the SI). This heterogeneous CaP formation occurred even though the initial solution was undersaturated with respect to hydroxyapatite, because the release of Ca^{2+} from the composite was locally sufficient to create super-saturated conditions in the mineral–hydrogel composites. The total amount of silicate released was also ∼60% of the theoretical total amount of silicate incorporated as CSH in the mineral–hydrogel composites, based on a mass balance of total silicate introduced into the solution from the mineral–hydrogel composites compared to the final silicate concentration in the aqueous solution. This finding precludes the possibility of phosphate adsorption to the CSH mineral seeds as a dominant mechanism for P removal. It is also worth noting that the final silicate concentrations we observed (∼9 mg-SiO_2/L) are in the range of ambient silica concentrations in surface streams and groundwater (∼14 mg-SiO_2/L and ∼17 mg-SiO_2/L, respectively).[34] Therefore, the amount of silicate release that we observed would not create a new concern.

https://doi.org/10.1021/acsestengg.1c00204
ACS EST Engg. XXXX, XXX, XXX−XXX

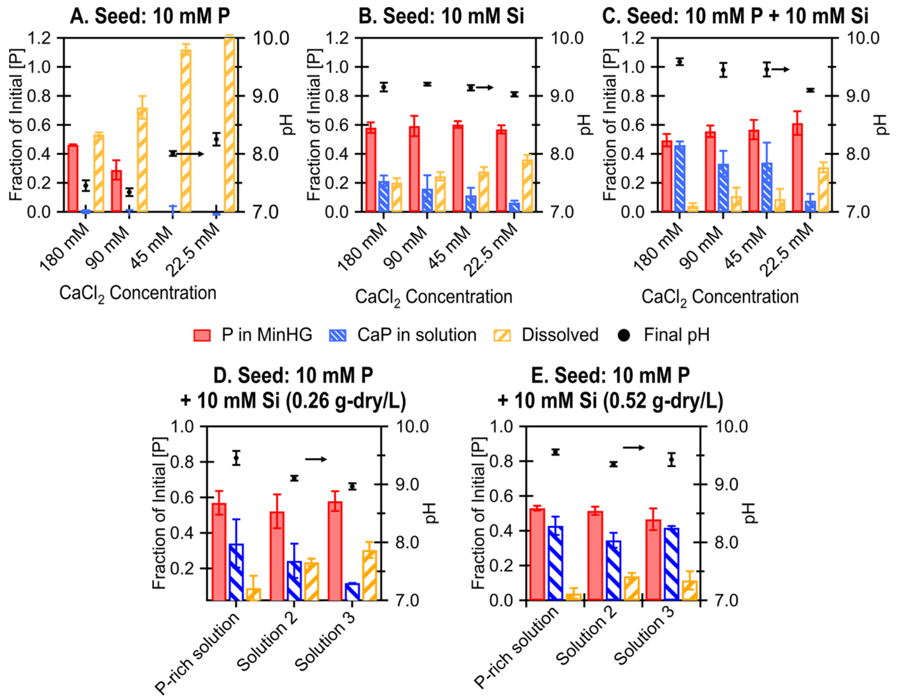

Figure 5. pH values and distributions of phosphate in P-rich solution batch reactions after 16 h of reaction with mineral−hydrogel composites formed from different calcium chloride batch concentrations, with seed minerals formed from ionic precursors of (A) 10 mM P, (B) 10 mM Si, and (C) 10 mM P + 10 mM Si. The amount of NaOH in the calcium bath was fixed at 20 mM NaOH for each concentration. All error bars are from triplicate measurements and represent 1 standard deviation. (D) Composite dose of0.26 g-dry hydrogel/L and (E) Composite dose of 0.52 g-dry hydrogel/L. Final pH values and P distributions of (D) and (E) after 16-h batch reactions in P-rich aqueous solution, P-rich aqueous solution with 1 mM $NaNO_3$ and 1 mM Na_2SO_4 (Solution 2 in (D) and (E)), and P-rich aqueous solution with 1 mM $NaNO_3$, 1 mM Na_2SO_4, and 2 mg-C/L dissolved organic matter (DOM) (Solution 3 in (D) and (E)). In (D) and (E), the mineral−hydrogel composites were made with a 45 mM $CaCl_2$ batch concentration.

The mechanisms and processes for silicate release and P removal and recovery are presented in Figure 4. We propose that two main processes are involved in P recovery by the mineral−hydrogel composites (Figure 4A). First, CSH mineral seeded composites release Ca^{2+} and $H_3SiO_4^-$ by dissolution. These ions then diffuse through the hydrogel to the outer solution. Simultaneously, P diffuses inward from the solution, creating a local microenvironment within the hydrogels that highly favors heterogeneous CaP nucleation and growth, the second process contributing to P recovery. The role of local microenvironments for P recovery through crystallization has been recently emphasized. For example, Lei et al. reported the importance of elevated pH near the cathode during electrochemical recovery of CaP.[35] Hovelmann and Putnis used atomic force microscopy to directly observe the nucleation and growth of struvite on a brucite ($Mg(OH)_2$) surface. The dissolution of brucite in their system created a boundary layer with a highly favorable environment for struvite formation.[36] Cunha et al. reported that CaP formation is favored in granules with an increased internal pH from biological activity.[37] In hydrogel systems, increased internal pH values have been engineered for the removal of heavy metal ions through selection of appropriate monomer units[38] or for the protection of pH-sensitive enzymes through the inclusion of brucite.[39] These engineered hydrogels were respectively applied to selectively recover metal ions and protect acid-sensitive compounds. In our system, we engineered an elevated internal pH through the inclusion of highly soluble CSH mineral seed within the hydrogel. The dissolution and diffusion of $H_3SiO_4^-$ through the hydrogel act as transport barriers to maintain a locally high internal pH.

To gain further insights into CaP formation and CSH dissolution, we estimated their stoichiometries (Figure 4B). While the exact stoichiometries of the mineral seeds and heterogeneously and homogeneously formed CaP minerals are unknown, they can be estimated by the known stoichiometries for amorphous CaP[40] and amorphous CSH.[41] For amorphous CSH, we use the reported stoichiometry for the highest Ca:Si ratio (2.2:1) to represent the CSH mineral seed, because it is the closest value to the Ca:Si ratio from dissolution of the mineral−hydrogel composites in 30 mM NaCl solution (Figure 3D).[41] Based on these equations, the dissolution of CSH can directly promote the growth of CaP seed through the release of Ca^{2+} and OH^-. Importantly, the hydrogel facilitates this process because it contains both mineral seeds near each other. The released silicate may also contribute to CaP nucleation and growth, both during mineral seed formation and phosphate recovery. Previously, low concentrations of silicate have been reported to increase the nucleation rate of hydroxyapatite in simulated body fluid and in neutral aqueous solutions.[42,43] Silicate can also potentially be incorporated into the CaP structure. This can potentially inhibit the crystallization of calcium phosphate, stabilizing the amorphous phase and making the mineral seeds more soluble and the phosphate more available for reuse applications.[31,42,43] Another potential possibility is that a silica shell/patch can form as reported by Wang et al., who observed this phenomenon during the precipitation of amorphous CaP in the presence of silicate,

https://doi.org/10.1021/acsestengg.1c00204
ACS EST Engg. XXXX, XXX, XXX−XXX

Table 1. Comparison of Our Mineral–Hydrogel Composites with Different CSH Mineral Seeds/Adsorbents Reported in the Literature[a]

seed material	particle size	lowest reported [P] from batch experiments and final pH	P loading at ~2.65 mg-P/L	ref
mineral seed in CSH+CaP/Ca-Alg mineral–hydrogel composite	~2 mm	0.25 mg-P/L; pH = 9.6	27.2 mg-P/g mineral seed	this study
porous CSH	~74 μm	2.16 mg-P/L; pH = 10.2	24.5 mg-P/g CSH	44
amorphous CSH	~19 μm	17.8 mg-P/L; pH = 8.6	14.1 mg-P/g CSH	15
porous CSH	~74 μm	0.15 mg-P/L; pH = 10	5.8 mg-P/g CSH	55
CSH powder immobilized in PVA hydrogel	1 cm × 1 cm sheets, thickness NR	<0.5 mg-P/L; pH = 9.4	8 mg-P/g CSH	46
CSH pellets bound by PVA and Ca-Alg	pellets (mm scale) (exact measurements not reported)	3.82 mg-P/L; pH = NR	0.59 mg-P/g CSH	47
CSH (tobermorite)	40–50 μm	0.47 mg-P/L; pH = 10.2	9.1 mg-P/g CSH	18
CSH (Sonochemical Synthesis)	80–150 μm	~2.6 mg-P/L; pH = 9.5–10.5	29.4 mg-P/g CSH	45

[a]P-loading at ~2.65 mg-P/L was either estimated from experimental data in published figures or calculated from the Langmuir equation constants referenced in the last column.

which might slow the release rate of phosphate from the mineral–hydrogel composites.[42]

Reduction of Calcium and Phosphate Addition Required for Composite Synthesis. Different fabrication parameters, such as the calcium chloride bath concentration, change the mineral seeds and its P removal and recovery performance, influencing the composites' performance. Thus, we tested varied calcium chloride bath concentrations (22.5 mM–180 mM) for the three different mineral seeds (CaP, CSH, CaP + CSH).

The calcium concentration mainly affected the solubility of the CaP mineral seed (Figure 5A). At 180 mM and 90 mM $CaCl_2$, the CaP mineral seeds were much less soluble than those formed in either a 45 mM $CaCl_2$ bath or a 22.5 mM $CaCl_2$ bath, as shown by the final dissolved phosphate levels after 16 h. The CSH mineral's characteristics were less affected, as evidenced by the consistent levels of P removal and the final pH level (Figure 5B). For the combined CaP + CSH seeds as shown in Figure 5C, the calcium chloride bath concentration mainly affected the amount of homogeneous nucleation and growth, with 180 mM $CaCl_2$ yielding the highest and 22.5 mM $CaCl_2$ yielding the lowest. This result indicates that the overall amount of calcium incorporated into the mineral seed is dependent on the $CaCl_2$ bath concentration, with higher concentrations incorporating more calcium. When the mineral–hydrogel composites are placed in the P-rich solution, the calcium is released, with more calcium causing more CaP mineral formation in the solution. However, for the combined CaP + CSH seeds, the amount of P removed by heterogeneous nucleation and the final dissolved P concentration were similar for all $CaCl_2$ concentrations. This aspect allows less $CaCl_2$ to be used in producing mineral–hydrogel composites, without affecting their removal and recovery performance. The Si ionic precursor also increases the supersaturation ratio during CaP mineral formation, producing a final CaP mineral seed that is less soluble with less phosphate compared to our previous work (10 mM compared to 35 mM).[19] The supersaturation of CaP is also crucial in fabricating the mineral–hydrogel composites, so decreasing either calcium or phosphate in the fabrication process is normally offset by increasing the other element. Adding silicate to the mineral–hydrogel composites decreases both elements simultaneously, lowering the overall materials requirement for synthesis. Furthermore, the mineral–hydrogel composites are synthesized at room temperature from an environmentally-benign polymer and abundant elements of calcium and silica, in accordance with the principles of green chemistry. Additionally, the release of P from the mineral–hydrogel composites for the 10 mM P mineral seed in the first cycle (Figure 3A,C) and the 10 mM Si mineral seed in the third cycle (Figure 3F) demonstrate that the P contained within the CaP mineral seed is recoverable by dissolution. This was also demonstrated in our previously published work, where we showed that P can be released in undersaturated aqueous conditions at a sufficient concentration for plant growth in a quartz powder column (simulating soil applications).[19]

Effect of Different Anions on CaP + CSH/CaAlg Mineral–Hydrogel Composites. To determine the effect of common anions on the P recovery and removal performance of the CaP + CSH/CaAlg mineral–hydrogel composites, we modified the P-rich solution to contain (1) 1 mM sodium nitrate and 1 mM sodium sulfate (Solution 2 in Figure 5D,E) or (2) 1 mM sodium nitrate, 1 mM sodium sulfate, and 2 mg-C/L dissolved organic matter (DOM) (Solution 3 in Figure 5D,E). We found that the presence of these anions and DOM mainly reduced the amount of homogeneous nucleation that occurs within the solution, whereas the heterogeneous nucleation amount was not affected. The final P concentrations are therefore higher than the final P concentration achieved when no competing anions are present (Figure 5D). We found that increasing the dose of mineral–hydrogel composite can compensate for this effect, achieving similar final concentrations of aqueous P (Figure 5E).

Comparison with Other Calcium Silicate-Based and Common P-Removal/Recovery Methods. To determine the relative P affinity and reactivity of the mineral–hydrogel composites, we compared our composites to previously reported P recovery technologies using CSH mineral seeds (Table 1). For a more direct comparison, we used P-loading (mg-P/g mineral seed) at an equilibrium concentration of 2.65 mg-P/L, the final concentration reached by CaP + CSH/Ca-Alg in HAP undersaturated conditions (Figure 3D). Overall, our mineral–hydrogel composites have three advantages over the currently reported CSH mineral-based P removal methods. First, our composites have comparable P reactivity to CSH mineral seeds reported recently as effective P recovery materials.[44,45] Both of these studies created highly reactive seed minerals or adsorbents by using either pore-forming agents or sonochemical synthesis, demonstrating that mineral seeds synthesized inside the hydrogel are highly reactive with respect to P uptake. However, our *in situ* mineral–hydrogel composite synthesis is simpler and less energy intensive.

https://doi.org/10.1021/acsestengg.1c00204
ACS EST Engg. XXXX, XXX, XXX–XXX

Second, the mineral–hydrogel composites are more reactive than similar materials that combined hydrogels with inorganic mineral seeds.[46,47] Both studies formed hydrogels around preformed CSH minerals. Their reduced reactivities can be attributed to transport limitations, commonly found in hydrogel adsorbent systems,[48] or to reduced mineral reactivity. In our mineral–hydrogel composites, we expect that transport limitations will be lower than in other systems, because the calcium bath gelation method should form mineral seeds close to the surface of the mineral–hydrogel composites. Third, our CaP + CSH mineral seed can be easily recovered because of the mineral–hydrogel composite's large millimeter-scale size. Therefore, they are easily recovered for potential application as fertilizers, as studied in our previous work.[19]

The CaP + CSH/Ca-Alg mineral–hydrogel composites also compare favorably with other reported P-targeting sorbents with regards to P-affinity. Here, we defined P-affinity as the P loading (mg-P/g) at a specified equilibrium concentration (q_e). If a composite has a higher q_e at the specified equilibrium concentration, it has a higher P-affinity. Based on a recent review that compiled 63 reported adsorbents and their Langmuir adsorption isotherm model parameters, our CaP + CSH/Ca-Alg mineral seed has a higher P-affinity at a concentration of 2.65 mg-P/L than 55 of the adsorbents[20] (Figure S7 in SI). Moreover, while it maintains one of highest P-affinities, our mineral–hydrogel composite achieves this without the use of rare earth elements such as lanthanum or yttrium, using only renewable or environmentally abundant materials such as alginate, calcium, phosphate, and silicate. The mineral–hydrogel composites developed here also show a great promise compared to other P removal/recovery technologies. Conventional precipitation by aluminum or iron salts can reliably achieve concentrations of ~1–2 mg-P/L. This performance is the range of the mineral–hydrogel composites, which achieved concentrations of 0.25 mg-P/L and 2.65 mg-P/L under hydroxyapatite supersaturated and undersaturated conditions, respectively. The mineral–hydrogel composites also have the added benefit of recovering usable phosphate, while iron phosphates and aluminum phosphates are generally not suitable for reuse.[49] Membrane technologies and biological phosphorus removal can also achieve low effluent phosphate levels, either alone or combined.[50,51] However, membrane fouling is a concern, and the microbial community needs to be monitored and maintained to sustain optimal phosphate removal. Another biological method to remove and recover phosphate involves the use of algae.[50] This approach is also promising; however, scaling up the system while maintaining the required illumination can be a challenge, whereas scaling up the mineral–hydrogel composites would require only increasing the amount of composite. Electrochemical systems using electrodes to induce CaP scaling, either alone or combined with biological processes, have also gained recent interest.[8,35,52,53] These systems require power and maintenance, such as electrode cleaning and replacement, whereas the mineral–hydrogel composites do not.

Overall, mineral–hydrogel composites share many benefits with adsorptive technologies and crystallization technologies, while also mitigating some of their weaknesses. Like adsorptive technologies, they are quickly and easily applied. Moreover, the use of CaP beneficially increases their P affinities, compared to commonly reported adsorbents. Like crystallization technologies, the recovered P is easily usable and in a stable mineral form. Furthermore, due to the prevalence of calcium, the CSH mineral seeds, and the templating ability of the CaP mineral seeds, no additional chemical dosing is required, as is common with crystallization technologies based on struvite or CaP. The mineral–hydrogel composites also can be applied directly to remediate phosphate-enriched water and easily collected, due to their large size and ease of P collection.

■ CONCLUSIONS

To remove and recover phosphate from aqueous solution, we developed new CaP + CSH/Ca-Alg mineral–hydrogel composites. By incorporating both P and Si into the precursor solution, we synthesized mineral–hydrogel composites composed of calcium alginate, CaP, and CSH. The mineral–hydrogel composites, when placed in the P-rich solution, quickly recovered phosphate, and their removal performance compared favorably with those of previously reported highly efficient P removal methods. The mineral–hydrogel composites create HAP-supersaturated conditions by releasing calcium, silicate, and hydroxide. In addition, the incorporation of Si into the mineral seeds lowers the amounts of calcium and phosphate used to fabricate the mineral–hydrogel composites, while maintaining favorable mineral seed properties for P recovery. This incorporation makes the fabrication process more economical and more resource efficient than its synthesis without Si incorporation. Furthermore, calcium alginate is biodegradable in soil, making the disposal and reuse of these mineral–hydrogel composites environmentally benign.[54]

Through changing the calcium bath concentration and the amounts and their ratios of ionic precursors, the underlying role of each process parameter in P recovery and removal was revealed. The Ca-Alg hydrogel played a key role in both mineral seed formation, by limiting the mineral seed size and amount of carbonate impurities, and in P recovery, by creating an aqueous environment that is highly favorable for CaP formation and growth. The millimeter-size mineral–hydrogel composites we reported here showed promising performance, and the method can be further optimized for application in both point source treatment and nutrient recovery or remediation of nutrient polluted waters. After use, because the P is recovered in the form of CaP mineral, the mineral–hydrogel composites can be applied either as a direct reuse fertilizer or as a feedstock of P for other processes, allowing the mineral–hydrogel composites to contribute to "greening" the phosphorus cycle. Moreover, because the mineral–hydrogel composites create a locally favorable environment for P recovery, minimum effort is needed to adjust the bulk solution composition. This study successfully demonstrates the mineral–hydrogel composites as a promising sustainable technology for phosphate removal and recovery. Important future developments will include regeneration procedures to improve the mineral–hydrogel's performance for multiple cycles, scale up, and implementation in more realistic aqueous conditions, optimization of the mineral seeds for different aqueous conditions and applications, and reuse of the mineral–hydrogel composites.

■ ASSOCIATED CONTENT

Supporting Information

The Supporting Information is available free of charge at https://pubs.acs.org/doi/10.1021/acsestengg.1c00204.

Table of experimental goals, conditions, and figures guide (Table S1), detailed weights and sizes of hydrogel

https://doi.org/10.1021/acsestengg.1c00204
ACS EST Engg. XXXX, XXX, XXX−XXX

mineral composites (Table S2), USAXS, SAXS, and WAXS measurement apparatus (Figure S1), detailed SEM-EDS images and spectra of mineral−hydrogel composites (Figure S2), SEM-EDS images and spectra of the mineral−hydrogel composites after the P removal reaction (Figure S3), zoomed out SEM-BSE image of CaP + CSH/Ca-Alg mineral−hydrogel composite (Figure S4), kinetics of silicate release from mineral−hydrogel composites (Figure S5), phosphate removal performance in hydroxyapatite undersaturated conditions (Figure S6), and phosphate affinity comparison with reported phosphate adsorbent technologies (Figure S7) (PDF)

AUTHOR INFORMATION

Corresponding Author

Young-Shin Jun − *Department of Energy, Environmental and Chemical Engineering, Washington University in St. Louis, St. Louis, Missouri 63130, United States;* orcid.org/0000-0003-4648-2984; Email: ysjun@seas.wustl.edu

Authors

Albern X. Tan − *Department of Energy, Environmental and Chemical Engineering, Washington University in St. Louis, St. Louis, Missouri 63130, United States;* orcid.org/0000-0003-3157-3197

Elizabeth Michalski − *Department of Energy, Environmental and Chemical Engineering, Washington University in St. Louis, St. Louis, Missouri 63130, United States*

Jan Ilavsky − *X-ray Science Division, Argonne National Laboratories, Lemont, Illinois 60439, United States*

Complete contact information is available at: https://pubs.acs.org/10.1021/acsestengg.1c00204

Notes

The authors declare no competing financial interest.

ACKNOWLEDGMENTS

This article was developed under Assistance Agreement No. 84008401 awarded by the United States Environmental Protection Agency to Professor Young-Shin Jun. It has not been formally reviewed by the EPA. The views expressed in this document are solely those of the authors of this article and do not necessarily reflect those of the Agency. The EPA does not endorse any products or commercial services mentioned in this publication. A.X.T. acknowledges support from the National Science Foundation Graduate Research Fellowship Program (Grant No. DGE-1745038). This research utilized the setup and resources in sector 9-ID-C of the Advanced Photon Source, a U.S. Department of Energy (DOE) Office of Science User Facility operated for the DOE Office of Science by Argonne National Laboratory under Contract No. DE-AC02-06CH11357. The Nano Research Facility (NRF) and Insititute of Materials Science & Engineering (IMSE) at Washington University in St. Louis provided their facilities for the experiments. The authors acknowledge Professor James C. Ballard for carefully reviewing the manuscript.

REFERENCES

(1) Maupin, M. A.; Ivahnenko, T. Nutrient Loadings to Streams of the Continental United States from Municipal and Industrial Effluent. *J. Am. Water Resour. Assoc.* **2011**, *47* (5), 950−964.

(2) Watson, S. B.; Miller, C.; Arhonditsis, G.; Boyer, G. L.; Carmichael, W.; Charlton, M. N.; Confesor, R.; Depew, D. C.; Höök, T. O.; Ludsin, S. A.; Matisoff, G.; McElmurry, S. P.; Murray, M. W.; Peter Richards, R.; Rao, Y. R.; Steffen, M. M.; Wilhelm, S. W. The re-eutrophication of Lake Erie: Harmful algal blooms and hypoxia. *Harmful Algae* **2016**, *56*, 44−66.

(3) U.S. EPA. *A Compilation of Cost Data Associated with the Impacts and Control of Nutrient Pollution*; 2015.

(4) Schindler, D. W.; Carpenter, S. R.; Chapra, S. C.; Hecky, R. E.; Orihel, D. M. Reducing Phosphorus to Curb Lake Eutrophication is a Success. *Environ. Sci. Technol.* **2016**, *50* (17), 8923−8929.

(5) Mayer, B. K.; Baker, L. A.; Boyer, T. H.; Drechsel, P.; Gifford, M.; Hanjra, M. A.; Parameswaran, P.; Stoltzfus, J.; Westerhoff, P.; Rittmann, B. E. Total Value of Phosphorus Recovery. *Environ. Sci. Technol.* **2016**, *50* (13), 6606−20.

(6) Mew, M. C. Phosphate rock costs, prices and resources interaction. *Sci. Total Environ.* **2016**, *542*, 1008−1012.

(7) Li, B.; Huang, H. M.; Boiarkina, I.; Yu, W.; Huang, Y. F.; Wang, G. Q.; Young, B. R. Phosphorus recovery through struvite crystallisation: Recent developments in the understanding of operational factors. *J. Environ. Manage.* **2019**, *248*, 109254.

(8) Law, K. P.; Pagilla, K. R. Phosphorus Recovery by Methods Beyond Struvite Precipitation. *Water Environ. Res.* **2018**, *90* (9), 840−850.

(9) Peng, L.; Dai, H.; Wu, Y.; Peng, Y.; Lu, X. A comprehensive review of phosphorus recovery from wastewater by crystallization processes. *Chemosphere* **2018**, *197*, 768−781.

(10) Liu, X. N.; Wang, J. Impact of calcium on struvite crystallization in the wastewater and its competition with magnesium. *Chem. Eng. J.* **2019**, *378*, 122121.

(11) Golubev, S. V.; Pokrovsky, O. S.; Savenko, V. S. Unseeded precipitation of calcium and magnesium phosphates from modified seawater solutions. *J. Cryst. Growth* **1999**, *205* (3), 354−360.

(12) Ferguson, J. F.; Jenkins, D.; Eastman, J. Calcium Phosphate Precipitation at Slightly Alkaline pH Values. *Journal (Water Pollution Control Federation)* **1973**, *45* (4), 620−631.

(13) Menar, A. B.; Jenkins, D. *Calcium phosphate precipitation in wastewater treatment*; Office of Research and Monitoring, U.S. Environmental Protection Agency: 1972; Vol. 2.

(14) Hermassi, M.; Valderrama, C.; Dosta, J.; Cortina, J. L.; Batis, N. H. Evaluation of hydroxyapatite crystallization in a batch reactor for the valorization of alkaline phosphate concentrates from wastewater treatment plants using calcium chloride. *Chem. Eng. J.* **2015**, *267*, 142−152.

(15) Okano, K.; Uemoto, M.; Kagami, J.; Miura, K.; Aketo, T.; Toda, M.; Honda, K.; Ohtake, H. Novel technique for phosphorus recovery from aqueous solutions using amorphous calcium silicate hydrates (A-CSHs). *Water Res.* **2013**, *47* (7), 2251−2259.

(16) Song, Y.; Weidler, P. G.; Berg, U.; Nüesch, R.; Donnert, D. Calcite-seeded crystallization of calcium phosphate for phosphorus recovery. *Chemosphere* **2006**, *63* (2), 236−243.

(17) Lee, C.-G.; Alvarez, P. J. J.; Kim, H.-G.; Jeong, S.; Lee, S.; Lee, K. B.; Lee, S.-H.; Choi, J.-W. Phosphorous recovery from sewage sludge using calcium silicate hydrates. *Chemosphere* **2018**, *193*, 1087−1093.

(18) Jiang, J. Q.; Wu, L. Preliminary study of calcium silicate hydrate (tobermorite) as crystal material to recovery phosphate from wastewater. *Desalin. Water Treat.* **2010**, *23* (1−3), 49−54.

(19) Kim, D.; Wu, T.; Cohen, M.; Jeon, I.; Jun, Y.-S. Designing the crystalline structure of calcium phosphate seed minerals in organic templates for sustainable phosphorus management. *Green Chem.* **2018**, *20* (2), 534−543.

(20) Kumar, P. S.; Korving, L.; van Loosdrecht, M. C. M.; Witkamp, G. J. Adsorption as a technology to achieve ultra-low concentrations of phosphate: Research gaps and economic analysis. *Water Res. X* **2019**, *4*, 100029.

(21) Okano, K.; Miyamaru, S.; Kitao, A.; Takano, H.; Aketo, T.; Toda, M.; Honda, K.; Ohtake, H. Amorphous calcium silicate

https://doi.org/10.1021/acsestengg.1c00204
ACS EST Engg. XXXX, XXX, XXX−XXX

hydrates and their possible mechanism for recovering phosphate from wastewater. *Sep. Purif. Technol.* **2015**, *144*, 63−69.
(22) Schneider, C. A.; Rasband, W. S.; Eliceiri, K. W. NIH Image to ImageJ: 25 years of image analysis. *Nat. Methods* **2012**, *9* (7), 671−675.
(23) Ilavsky, J. Nika: software for two-dimensional data reduction. *J. Appl. Crystallogr.* **2012**, *45* (2), 324−328.
(24) Ilavsky, J.; Jemian, P. R. Irena: tool suite for modeling and analysis of small-angle scattering. *J. Appl. Crystallogr.* **2009**, *42* (2), 347−353.
(25) Ilavsky, J.; Zhang, F.; Andrews, R. N.; Kuzmenko, I.; Jemian, P. R.; Levine, L. E.; Allen, A. J. Development of combined microstructure and structure characterization facility for in situ and operando studies at the Advanced Photon Source. *J. Appl. Crystallogr.* **2018**, *51* (3), 867−882.
(26) Council, N. R. *Use of Reclaimed Water and Sludge in Food Crop Production*; The National Academies Press: Washington, DC, 1996; p 192.
(27) Doyle, J. D.; Parsons, S. A. Struvite formation, control and recovery. *Water Res.* **2002**, *36* (16), 3925−3940.
(28) U.S. EPA. *Case Studies on Implementing Low-Cost Modifications to Improve Nutrient Reduction at Wastewater Treatment Plants*; 2015.
(29) Jack, J.; Huggins, T. M.; Huang, Y. P.; Fang, Y. F.; Ren, Z. J. Production of magnetic biochar from waste-derived fungal biomass for phosphorus removal and recovery. *J. Cleaner Prod.* **2019**, *224*, 100−106.
(30) Solonenko, A. P.; Blesman, A. I.; Polonyankin, D. A. Poorly crystallized hydroxyapatite and calcium silicate hydrate composites: Synthesis, characterization and soaking in simulated body fluid. *Mater. Charact.* **2020**, *161*, 110158.
(31) Mostafa, N. Y.; Hassan, H. M.; Abd Elkader, O. H. Preparation and Characterization of Na+, SiO44-, and CO32-Co-Substituted Hydroxyapatite. *J. Am. Ceram. Soc.* **2011**, *94* (5), 1584−1590.
(32) Cao, X.; Harris, W. Carbonate and Magnesium Interactive Effect on Calcium Phosphate Precipitation. *Environ. Sci. Technol.* **2008**, *42* (2), 436−442.
(33) Burns, J. L.; Yan, Y.-D.; Jameson, G. J.; Biggs, S. A Light Scattering Study of the Fractal Aggregation Behavior of a Model Colloidal System. *Langmuir* **1997**, *13* (24), 6413−6420.
(34) Davis, S. N. Silica in streams and ground water. *Am. J. Sci.* **1964**, *262* (7), 870−891.
(35) Lei, Y.; Song, B.; Van Der Weijden, R. D.; Saakes, M.; Buisman, C. J. N. Electrochemical Induced Calcium Phosphate Precipitation: Importance of Local pH. *Environ. Sci. Technol.* **2017**, *51* (19), 11156−11164.
(36) Hovelmann, J.; Putnis, C. V. In Situ Nanoscale Imaging of Struvite Formation during the Dissolution of Natural Brucite: Implications for Phosphorus Recovery from Wastewaters. *Environ. Sci. Technol.* **2016**, *50* (23), 13032−13041.
(37) Cunha, J. R.; Tervahauta, T.; Van Der Weijden, R. D.; Temmink, H.; Hernández Leal, L.; Zeeman, G.; Buisman, C. J. N. The Effect of Bioinduced Increased pH on the Enrichment of Calcium Phosphate in Granules during Anaerobic Treatment of Black Water. *Environ. Sci. Technol.* **2018**, *52* (22), 13144−13154.
(38) Gotoh, T.; Sano, M.; Nakai, S. Selective Recovery of Metal Ion by Using Hydrogel With Different Inner pH. *Macromol. Symp.* **2019**, *385* (1), 1800163.
(39) Zhang, Z.; Chen, F.; Zhang, R.; Deng, Z.; McClements, D. J. Encapsulation of Pancreatic Lipase in Hydrogel Beads with Self-Regulating Internal pH Microenvironments: Retention of Lipase Activity after Exposure to Gastric Conditions. *J. Agric. Food Chem.* **2016**, *64* (51), 9616−9623.
(40) Combes, C.; Rey, C. Amorphous calcium phosphates: Synthesis, properties and uses in biomaterials. *Acta Biomater.* **2010**, *6* (9), 3362−3378.
(41) Nonat, A. The structure and stoichiometry of C-S-H. *Cem. Concr. Res.* **2004**, *34* (9), 1521−1528.
(42) Wang, Y.-N.; Jiang, S.; Pan, H.; Tang, R. Less is more: silicate in the crystallization of hydroxyapatite in simulated body fluids. *CrystEngComm* **2016**, *18* (3), 379−383.
(43) Tanizawa, Y.; Suzuki, T. Effects of silicate ions on the formation and transformation of calcium phosphates in neutral aqueous solutions. *J. Chem. Soc., Faraday Trans.* **1995**, *91* (19), 3499.
(44) Guan, W.; Ji, F.; Chen, Q.; Yan, P.; Zhang, Q. Preparation and phosphorus recovery performance of porous calcium−silicate−hydrate. *Ceram. Int.* **2013**, *39* (2), 1385−1391.
(45) Zhang, Z.; Wang, X.; Zhao, J. Phosphate recovery from wastewater using calcium silicate hydrate (C-S-H): sonochemical synthesis and properties. *Environmental Science: Water Research & Technology* **2019**, *5* (1), 131−139.
(46) Ding, S.; Fang, D.; Pang, Z.; Luo, B.; Kuang, L.; Wang, H.; Zhang, Q.; Shen, Q.; Ji, F. Immobilization of powdery calcium silicate hydrate via PVA covalent cross-linking process for phosphorus removal. *Sci. Total Environ.* **2018**, *645*, 937−945.
(47) Rallapalli, P. B. S.; Ha, J. H. Preparation of Calcium Silicate Hydrate Extrudates and Their Phosphate Adsorption Studies. *Applied Chemistry for Engineering* **2019**, *30*, 562−568.
(48) Khan, M.; Lo, I. M. C. A holistic review of hydrogel applications in the adsorptive removal of aqueous pollutants: Recent progress, challenges, and perspectives. *Water Res.* **2016**, *106*, 259−271.
(49) De-Bashan, L. E.; Bashan, Y. Recent advances in removing phosphorus from wastewater and its future use as fertilizer (1997−2003). *Water Res.* **2004**, *38* (19), 4222−4246.
(50) Bunce, J. T.; Ndam, E.; Ofiteru, I. D.; Moore, A.; Graham, D. W. A Review of Phosphorus Removal Technologies and Their Applicability to Small-Scale Domestic Wastewater Treatment Systems. *Front. Environ. Sci.* **2018**, DOI: 10.3389/fenvs.2018.00008.
(51) Xie, M.; Shon, H. K.; Gray, S. R.; Elimelech, M. Membrane-based processes for wastewater nutrient recovery: Technology, challenges, and future direction. *Water Res.* **2016**, *89*, 210−221.
(52) Kelly, P. T.; He, Z. Nutrients removal and recovery in bioelectrochemical systems: A review. *Bioresour. Technol.* **2014**, *153*, 351−360.
(53) Zhang, Y.; Desmidt, E.; Van Looveren, A.; Pinoy, L.; Meesschaert, B.; Van Der Bruggen, B. Phosphate Separation and Recovery from Wastewater by Novel Electrodialysis. *Environ. Sci. Technol.* **2013**, *47* (11), 5888−5895.
(54) Ertesvag, H. Alginate-modifying enzymes: biological roles and biotechnological uses. *Front. Microbiol.* **2015**, *6* (523), 523.
(55) Fang, D.; Huang, L.; Fang, Z.; Zhang, Q.; Shen, Q.; Li, Y.; Xu, X.; Ji, F. Evaluation of porous calcium silicate hydrate derived from carbide slag for removing phosphate from wastewater. *Chem. Eng. J.* **2018**, *354*, 1−11.

https://doi.org/10.1021/acsestengg.1c00204
ACS EST Engg. XXXX, XXX, XXX−XXX